



UNIVERSITY OF LEEDS

This is a repository copy of *Widespread seasonal speed-up of west Antarctic Peninsula glaciers from 2014 to 2021*.

White Rose Research Online URL for this paper:

<https://eprints.whiterose.ac.uk/196885/>

Version: Accepted Version

---

**Article:**

Wallis, BJ, Hogg, AE orcid.org/0000-0002-6441-4937, van Wessem, JM et al. (2 more authors) (2023) Widespread seasonal speed-up of west Antarctic Peninsula glaciers from 2014 to 2021. *Nature Geoscience*, 16 (3). pp. 231-237. ISSN 1752-0894

<https://doi.org/10.1038/s41561-023-01131-4>

---

© The Author(s), under exclusive licence to Springer Nature Limited 2023. This is an author produced version of an article published in *Nature Geoscience*. Uploaded in accordance with the publisher's self-archiving policy.

**Reuse**

Items deposited in White Rose Research Online are protected by copyright, with all rights reserved unless indicated otherwise. They may be downloaded and/or printed for private study, or other acts as permitted by national copyright laws. The publisher or other rights holders may allow further reproduction and re-use of the full text version. This is indicated by the licence information on the White Rose Research Online record for the item.

**Takedown**

If you consider content in White Rose Research Online to be in breach of UK law, please notify us by emailing [eprints@whiterose.ac.uk](mailto:eprints@whiterose.ac.uk) including the URL of the record and the reason for the withdrawal request.



[eprints@whiterose.ac.uk](mailto:eprints@whiterose.ac.uk)  
<https://eprints.whiterose.ac.uk/>

# 1 Widespread seasonal speed-up of west Antarctic Peninsula 2 glaciers from 2014 to 2021

3 Benjamin J. Wallis\*<sup>1</sup>, Anna E. Hogg<sup>1</sup>, J. Melchior van Wessem<sup>2</sup>, Benjamin J. Davison<sup>1</sup>, Michiel R.  
4 van den Broeke<sup>2</sup>

5 <sup>1</sup>School of Earth and Environment, University of Leeds, UK; <sup>2</sup>Institute for Marine and Atmospheric  
6 Research, Utrecht University, NL

7 \*Corresponding author E-mail: eebjwa@leeds.ac.uk

## 8 **Abstract**

9 Mass loss from the Antarctic Ice Sheet is dominated by ice dynamics, where ocean-driven melt leads  
10 to un-buttressing and ice flow acceleration. Long-term ice speed change has been measured in  
11 Antarctica over the past four decades; however, there are limited observations of significant short-term  
12 seasonal speed variability on the grounded ice sheet. Here we assess seasonal variations from in ice  
13 flow speed on 105 glaciers on the west Antarctic Peninsula using Sentinel-1 satellite observations  
14 spanning 2014 to 2021. We find an average summer speed-up of  $12.4 \pm 4.2$  %, with maximum speed  
15 change of up to  $22.3 \pm 3.2$  % on glaciers with the most pronounced seasonality. Our results show that  
16 over the six-year study period, glaciers on the west Antarctic Peninsula respond to seasonal forcing in  
17 the ice-ocean-atmosphere system, indicating sensitivity to changes in terminus position, surface melt  
18 plus rainwater flux and ocean temperature. Seasonal speed variations must be accounted for when  
19 measuring the mass balance and sea level contribution of the Antarctic Peninsula, and studies must  
20 establish the future evolution of this previously undocumented signal under climate warming scenarios.

## 21 **Main**

22 Over the past 25-years the Antarctic Ice Sheet contributed  $7.6 \pm 3.9$  mm to global sea level rise (SLR),  
23 with a four-fold increase in the rate of mass loss observed since 1992<sup>1</sup>. In Antarctica, mass loss is  
24 dominated by ice dynamic processes<sup>2</sup>, where acceleration of marine-terminating ice streams is driven

25 by a reduction in resistive force due to ocean-driven ice shelf thinning<sup>3-7</sup>, ice shelf disintegration<sup>8</sup>,  
26 terminus retreat<sup>9,10</sup> and increasing ice damage<sup>11</sup>. Ice speed measurements are a critical dataset for i)  
27 mass balance calculations using the input-output method<sup>12-14</sup>; ii) calibration of models used for  
28 projections of future ice sheet evolution<sup>15-17</sup>; and iii) studies to improve our understanding of the  
29 physical processes driving ice dynamics and ice-ocean-atmosphere interactions<sup>18,19</sup>. Therefore,  
30 generating accurate, high spatial and temporal resolution measurements of this important parameter is  
31 essential.

32 Satellite measurements have documented long-term, multi-year change in ice speed across Antarctica,  
33 with the largest accelerations observed in the Amundsen Sea sector<sup>10,14</sup>, the Getz basin<sup>20</sup> and on the  
34 Antarctic Peninsula (AP)<sup>9,21-23</sup>. However, ice speed can also vary on intra-annual timescales. In  
35 Greenland, seasonal ice velocity variations are widespread, caused by basal lubrication from the routing  
36 of surface meltwater, and at marine-terminating outlet glaciers in response to change in submarine melt  
37 rates and terminus position<sup>24-28</sup>. However, on the Antarctic Ice Sheet there are few observations of  
38 significant widespread seasonal changes in grounded ice speed. Reports of seasonality have been so far  
39 limited to two floating ice tongues in East Antarctica<sup>29,30</sup> and glaciers feeding the George VI Ice Shelf<sup>31</sup>.

40 Over the last three decades, the AP has experienced significant change. Floating ice shelves have  
41 collapsed and retreated<sup>32-34</sup>, and the loss of ice shelf buttressing strength has led to an acceleration in  
42 ice speed and surface lowering on the grounded ice, increasing ice discharge into the ocean<sup>9,13,35</sup>.  
43 Analysis of sediment cores shows that this change is significant on the geological timescale, with events  
44 of this magnitude not recorded on the AP since the mid Holocene, or in the case of Larsen-B, pre-  
45 Holocene<sup>36-38</sup>. Overall, AP glaciers north of 70°S have the potential to increase global mean sea level  
46 by  $69 \pm 5$  mm<sup>39</sup>, with 7.8 % (17,900 km<sup>2</sup>) of the AP glaciers thought to be in a state of dynamic  
47 imbalance in 2017<sup>40</sup>.

48 The mechanisms driving long-term change on the AP have been attributed to both atmospheric and  
49 ocean forcing, with different processes having greater relative importance in different regions. Increased  
50 near-surface air temperatures were recorded on the AP in the second half of the 20<sup>th</sup> century and linked  
51 to ice shelf retreat<sup>41</sup>; however, extending the temperature record into the 21<sup>st</sup> century shows that the

52 warming trend was replaced by a statistically significant period of atmospheric cooling from 1999 to  
53 2014<sup>42</sup>. Despite this long-term cooling trend, air temperatures exceed 0°C in the summer months  
54 causing widespread surface melt and significant rain<sup>43-45</sup>. Warm deep ocean water has been linked to  
55 terminus retreat on the western AP<sup>46</sup>, ice speed increase on the English Coast<sup>47</sup>, and grounding line  
56 retreat on Fleming Glacier<sup>21</sup>. Attribution of causal processes is complex as different forcing mechanisms  
57 can dominate at different time periods. On the AP, the role of surface melt driven velocity fluctuations  
58 has been debated<sup>31,48,49</sup>. Three instances of short-lived (<6 days) speed change were observed  
59 simultaneously on four east and one west AP glaciers between October 2016 and April 2018<sup>48</sup>. This  
60 was attributed separately to both the lubrication of ice flow following surface meltwater drainage<sup>48</sup>, and  
61 a surface-melt induced velocity processing artefact and ocean dynamic forcing<sup>49</sup>. Consequently, further  
62 studies are required to improve our understanding of the ice flow response to changing environmental  
63 conditions in this region. In this study, we use satellite observations to produce a 6-year long record of  
64 ice speed measurements on 105 glaciers on the west AP coast, north of George VI Ice Shelf (Fig. 1a).

## 65 **Seasonal Change in Ice Speed**

66 Our observations show the spatial distribution of ice velocity across the west AP at 100 m posting (Fig.  
67 1a). We extracted time-series of ice speed on 105 glaciers at a location 1 km up-stream of the terminus  
68 position, which shows an average ice speed of 998 m/yr and 26 glaciers flowing at speeds of over 1.5  
69 km/yr. Fast ice flow above 1 km/yr, extends up to 18 km inland on major outlets such as Fleming and  
70 Cayley Glaciers, and ice flow is well resolved across the full width of smaller ~1 km wide flow units  
71 with small-scale velocity features such as tributaries also resolved. The ice speed autocorrelation metric,  
72 a measure of annual periodicity, shows high values across the west AP, with the largest density of  
73 summer speed-up found on glaciers at northern latitudes (Fig. 1b). The ice speed interquartile range  
74 indicates the amplitude of the change (Fig. S2b). This shows that the highest amplitude seasonal  
75 variability is observed on glaciers on the Davis Coast, located to the north of Brabant Island, and near  
76 Anvers Island, with different amplitudes of variability observed on neighboring glaciers. Heterogeneity  
77 in the timing and magnitude of speed change between neighboring glaciers is expected, and has been  
78 observed extensively in Greenland and Antarctica<sup>25,28,50,51</sup>.

79 Our velocity time-series reveals that seasonal variability in ice speed is widespread across the west AP  
80 coast, with a mean summer speed-up of over 10 % measured on 76 of the 105 glaciers in the study  
81 region (Fig. 2, Fig. S2). Excluding the 27 glaciers which flow at speeds less than 500 m/yr to avoid  
82 undue influence from other sources of small-scale variability, such as measurement noise, we observe  
83 a mean intra-annual speed variability of  $124.2 \pm 42.2$  m/yr on the west AP, equivalent to a  $12.4 \pm 4.2$   
84 % speed-up during the austral summer. The strongest seasonal cycle is observed on Hotine Glacier (Fig.  
85 2d), located on the Kyiv Peninsula, which speeds-up on average by  $22.3 \pm 3.2$  % ( $288.3 \pm 41.3$  m/yr)  
86 in the summer months compared to its winter minimum. Other glaciers observed to have an extremely  
87 pronounced seasonal velocity cycle include the unnamed North Bone Bay Glacier which experienced a  
88 mean summer speedup of  $20.2 \pm 3.4$  % ( $125.6 \pm 21.2$  m/yr) (Fig. 2a), Gavin Ice Piedmont  $6.6 \pm 3.1$  %  
89 ( $211.2 \pm 98.7$  m/yr) (Fig. 2b), Leonardo Glacier  $18.3 \pm 2.7$  % ( $212.7 \pm 31.5$  m/yr) (Fig. 2c), Trooz  
90 Glacier  $5.8 \pm 2.4$  % ( $123.6 \pm 50.5$  m/yr) (Fig. 2e) and Keith Glacier  $6.6 \pm 3.3$  % ( $107.8 \pm 54.2$  m/yr)  
91 (Fig. 2f) respectively. On the glaciers shown in Figures 2a-f, seasonal ice speed variability is observed  
92 between 2 km and 5 km inland of the terminus (Fig. S4).

### 93 **Long-term Ice Dynamic Response**

94 In addition to widespread short-term seasonal ice speed variability our results also show newly observed  
95 longer-term, multi-annual ice dynamic signals on west AP glaciers. Most significantly, Cadman Glacier  
96 (Fig. 2g) located in Beascochea Bay accelerated by  $1.05 \pm 0.07$  km/yr ( $42.9 \pm 2.7$  %) in 2019.  
97 Splettstoesser Glacier located on the Stresher Peninsula exhibited a multiyear slowdown of  $315 \pm 20$   
98 m/yr ( $35.9 \pm 2.3$  %) over the full 6-year study period; and Otlet Glacier which flows into the Grandidier  
99 Channel, experienced a multi-year acceleration of  $278 \pm 26$  m/yr ( $38.4 \pm 3.6$  %) between 2014 and  
100 2021. While Fleming Glacier exhibits a clear seasonal ice speed signal, our velocity time-series shows  
101 that this is imposed on top of the longer-term ice dynamic trend (Fig. 2h) which reached its peak speed  
102 of 2.9 km/yr in 2012<sup>21</sup>.

## 103 **Influence of External Forcing Mechanisms**

104 We investigated the influence of external forcing mechanisms and change in calving front location on  
105 eight highlight glaciers which are spatially distributed across the study area (Figs. 1b, 2a to h). Glaciers  
106 with pronounced seasonal ice speed variability during the study period were selected (Figs. 2a to f),  
107 along with regions where a longer-term ice dynamic response was observed, as seen on Cadman (Fig.  
108 2g) and Fleming Glaciers (Fig. 2h).

109 We assessed the availability of surface water on the west AP by extracting daily estimates of snowmelt  
110 and rainfall from a regional climate model (RACMO2.3p2)<sup>43,45,52</sup> (Figs. 2a to h). The results show that  
111 on the AP the summer melt season lasts 4 to 5 months, with snowmelt starting in October and peaking  
112 in December and January. Significant late-season surface melt days occur throughout February and in  
113 some areas into March. This is consistent with microwave scatterometer and modelling studies showing  
114 persistent melt durations in excess of 100 days on the AP<sup>44</sup>. Larger volumes of surface melt and  
115 precipitation are found at the northern tip of the AP<sup>43</sup>, where seasonal speed variations were strongest  
116 (Fig. 1b, Fig S2b). Rainfall in the late-austral summer (Jan to April), extends the period where liquid  
117 water is available at a time when other sources of surface-derived melt water are decreasing. Our results  
118 show that on the six highlight glaciers with pronounced seasonal ice speed variability, the seasonal  
119 speed-up roughly coincided with the onset of surface melting each year, however, the highest ice speeds  
120 generally occur several weeks after the peak in surface water supply (Figs. 2a to f, Fig. 3). Further  
121 analysis of modelled runoff at the basin scale shows that on the west AP, runoff lags surface meltwater  
122 and rain flux by several weeks (Fig. S5) and peaks in February for the period July 2016 – July 2021,  
123 coinciding directly with the peak in ice speed (Fig. 3). We therefore attribute this lag to the time taken  
124 for the water to percolate through the firn layer of the west AP, which can be up to 100m thick<sup>53</sup>.  
125 Modelling predicts the presence of perennial firn aquifers on the west AP<sup>54</sup>, which may provide a  
126 mechanism for modulating the supply of meltwater to the bed throughout the year. On the 20 glaciers  
127 with the strongest annual ice speed periodicity (highest autocorrelation values), we recorded the largest  
128 average seasonal speed variability ( $167.4 \pm 40.0$  m/yr) during our study period in the 2019/2020 austral  
129 summer when record high surface melt was observed on the AP<sup>55</sup>. This indicates that the largest

130 seasonal speed-up occurs in years with most surface melt. The spatial distribution of strong surface melt  
131 and the temporally coincident peak in runoff with the highest annual summer speeds indicates a link  
132 between hydrologically driven basal lubrication on west AP glaciers.

133 Ocean temperature data from a reanalysis model<sup>56</sup> were used to assess the spatially variable pattern of  
134 integrated ocean heat variability in the top 110 m of the water column in the Bellingshausen Sea,  
135 between 2015 and 2020 (Fig. 1b). Our results show that there is a strong seasonal signal in the  
136 temperature anomaly, with mean seasonal variability of 1.9 °C recorded in the Bellingshausen Sea north  
137 of Adelaide Island, and maximum local change of up to 3.1 °C found at the tip of the AP north of the  
138 Davis Coast (Fig. 1b). Our ice speed time-series show that on seven of the eight highlight glaciers there  
139 is a strong correspondence between the timing of the seasonal ice speedup and ocean temperature  
140 increase (Figs. 2a to g). The exception to this is in Marguerite Bay next to Fleming Glacier where there  
141 is no strong seasonality in the ocean temperature anomaly (Fig. 2h). Previous studies have shown that  
142 persistent sea-ice cover in this area<sup>57</sup> acts as a thermal barrier, preventing warming of surface waters in  
143 the summer and heat loss to the atmosphere in the winter, as observed previously in Ryder Bay<sup>58</sup>.

## 144 **Change in Calving Front Location**

145 We exploited the full Sentinel-1 archive to measure change in terminus position on all eight highlight  
146 glaciers throughout the 6-year study period (Figs. 2a to h)<sup>59</sup>. In all cases, we observe seasonal variability  
147 in the terminus position with maximum advance in winter or early spring and retreat during the summer,  
148 with the most pronounced change in terminus position observed on slower flowing glaciers (Fig. 2a &  
149 2c). On the six glaciers with strong seasonal ice speed periodicity (Figs. 2a to f) the terminus position  
150 retreated inland during the summer months by 117 m on average, with a minimum and maximum  
151 summer retreat of 35 m and 254 m measured on Gavin Ice Piedmont and Trooz Glacier respectively.

152 We observed a multi-annual change in terminus position on Cadman Glacier where the terminus  
153 retreated by 10 km over a 2-year period, between its most advanced position in February 2019 and the  
154 final measured position in May 2021 (Fig. 2e). This change corresponded with a major and sustained  
155 1.04 km/yr (42.0 %) increase in ice speed that started in October 2018. The observed speed-up started

156 two months prior to the onset of sustained terminus retreat, suggesting that an un-buttressing occurred  
157 first, followed by the resulting acceleration and terminus retreat. Our results show that Fleming Glacier  
158 experienced a pattern of winter terminus advance and summer retreat caused by large calving events  
159 over the 6-year study period. In 2020 the peak summer speed of 2.43 km/yr was recorded in April  
160 following a 2.16 km calving front retreat event in February 2020 (Fig 2h). This suggests that the speed  
161 of Fleming Glacier is significantly dependant on the terminus position, on intra-annual timescales, with  
162 sensitivity to change enhanced by its retrograde bed slope geometry<sup>21,60</sup>.

## 163 **Discussion**

164 We further assessed the role of external forcing mechanisms as a driver of seasonal change by  
165 comparing the monthly distribution of annual maximum and minimum ice speeds on all 105 glaciers,  
166 with the monthly distribution of mean surface water flux and ocean temperature anomaly averaged  
167 across the full period of data availability (Fig. 3). The results show a clear seasonal distribution of both  
168 ice speed and external forcing over the whole west AP study region, with speed minimums recorded  
169 between September and October each year before the summer season starts, and maximum speeds  
170 occurring from February to April each year when surface water supply and ocean temperature are  
171 higher. This shows that either individually or in combination, meltwater-induced changes in basal  
172 effective pressure and ocean-temperature induced changes in terminus ablation rates, are at least  
173 partially responsible for the observed changes in ice speed. At seven of the eight highlight glaciers, we  
174 also find a clear correspondence between seasonal terminus position change, potentially driven by ocean  
175 temperature changes, and ice speed (Figs. 2a to g). This monthly distribution is even more pronounced  
176 if only the 20 glaciers with the strongest annual periodicity in ice speed are assessed (Fig. 3).

177 While the size of a glaciers ice dynamic response will be in-part controlled by the strength of the  
178 environmental forcing, the sensitivity of an individual glacier to respond is controlled by glacier  
179 geometry<sup>61</sup> and subglacial conditions<sup>50</sup>. Mechanistically, the observed seasonal speed fluctuations must  
180 be driven by changes in buttressing force and/or basal sliding. On seasonal timescales, the buttressing  
181 force can be reduced by terminus retreat during the summer, however, this must itself be driven by an



182 increase in ice front ablation caused by environmental factors. In Svalbard and the AP, upper ocean  
183 temperature is strongly linked to high rates of ablation at the terminus of tidewater glaciers<sup>62,63</sup>. Our  
184 results show that glaciers with the largest seasonal speed variability undergo significant terminus  
185 position change and are adjacent to ocean water with the greatest seasonal ocean temperature variability  
186 which is strongest at the northern tip of the west AP (Fig. 1b) (Figure 2a-f). This provides a mechanism  
187 for seasonal ice speed fluctuations on the west AP to be forced by ocean temperature induced frontal  
188 retreat.

189 Meltwater penetration to the glacier bed can reduce basal traction and cause hydraulic jacking, both of  
190 which induce ice speed-up. Our regional climate model results show high summertime water flux at the  
191 surface corresponding to observations of summertime ice speed-up, and that a lag between the peak  
192 surface melt and peak summer ice speed-up can be explained by the time required for surface water to  
193 percolate through the snowpack as runoff (Fig. 3). Interannual variability in the magnitude of seasonal  
194 speed-up may also be explained by surface water availability, as the year with the most surface melt  
195 (2019/20) coincided with the year with the largest seasonal speed-up on many glaciers in the study area.  
196 Sparse field studies have observed glacial sediment plumes on the west AP coast, providing further  
197 evidence that meltwater reaches the subglacial drainage system in this region<sup>64,65</sup>. While future studies  
198 must seek to partition the relative importance of different forcing mechanisms on individual glaciers,  
199 we can conclude that the seasonal ice speed changes we observe on the west AP are due to increased  
200 heat in the ice-atmosphere-ocean system forcing glacier dynamics.

201 Our results are important for mass balance studies where the input-output method is used<sup>1,13</sup>, because  
202 seasonal change in ice speed causes a seasonal variation in ice discharge. If summer ice speed is  
203 assumed to be representative of the annual mean, this leads to an overestimation of the ice discharge  
204 and consequently a negative bias in the mass balance assessments. We quantify the impact of this bias  
205 on mass balance by calculating ice discharge for the six highlight glaciers (Fig 2a-f), using the full time  
206 series of seasonally variable ice speed, and with a linear interpolation between summer maximum  
207 speeds. Our results show that for these glaciers, when summer speeds alone are used the ice discharge

208 is overestimated by 7.2 % on average, with the mass balance 30.2 % more negative than it would be if  
209 seasonal speed variability is accounted for (Table S1).

210 We observe strong seasonal flow variability during our 6-year study period, but our results do not show  
211 the timing of its onset. The AP experienced the greatest warming of any Southern Hemisphere terrestrial  
212 region in the latter twentieth century<sup>66,67</sup>, however, air temperatures decreased from the late 1990's to  
213 2014<sup>42</sup>. Surface water flux data from RACMO shows that between 1979 and 2019, meltwater forcing  
214 has been at current or higher levels throughout the 40-year period, suggesting seasonal ice speed  
215 changes on the west AP could have been present in previous decades. In the future, atmospheric  
216 temperatures on the AP are projected to rise under a 1.5°C warming scenario<sup>67</sup>, the availability of  
217 surface meltwater is projected to double by 2050 independent of the climate scenario<sup>68</sup>, and precipitation  
218 is projected to increase<sup>69</sup>; all affecting the seasonal forcing applied to glaciers in the region and their  
219 mass balance. Future studies should combine in-situ measurements with satellite observations to further  
220 investigate the complex link between ice speed, surface melt and ocean temperature variability across  
221 the west AP, and to assess their relative importance at the glacier basin scale. Long and short-term ice  
222 dynamic trends must be monitored and understood, with the large number of AP glaciers and the variety  
223 of responses providing a natural laboratory that can be used to improve our understanding of the  
224 processes driving present-day ice loss in Antarctica. Substantial differences remain between estimates  
225 of the sea level contribution from the AP made using independent techniques<sup>1</sup>, and our results show  
226 that accounting for seasonal speed variations may enable a proportion of that difference to be reconciled.

## 227 **Figure Captions**

228 **Figure 1 – West Antarctic Peninsula ice speed map and ice speed autocorrelation.**

229 (a) Mean ice speed (km/yr) on the west Antarctic Peninsula (Dec 2014 – May 2021). (b) Glacier  
230 drainage basins<sup>70</sup> shaded by the autocorrelation statistic (Dec 2014 – May 2021), which indicates high  
231 (red) and low (light grey) annual periodicity in ice speed. Inter-annual upper ocean temperature  
232 variation is also shown, measured as the annual interquartile range of the depth averaged temperature  
233 anomaly from the top 110 m of the water column (2015 – 2020)<sup>56</sup>. The REMA Antarctica 200 m DEM

234 hill- shade<sup>71</sup>, coastline (black line) and hill-shade bathymetry from IBSCO v1<sup>72</sup> are shown on both maps  
235 for illustrative purposes. Time -series are shown in Figure 2a-h for glaciers highlighted a-h.

236 **Figure 2a to h – Highlight glaciers time series of ice speed, surface water flux, terminus position**  
237 **and ocean temperature anomaly.**

238 Time-series of Kalman smoothed ice speed (black solid line), RACMO2.3p2 surface water flux (snow  
239 melt plus rain) (blue dots)<sup>43,52</sup> terminus position with respect to the final position (green solid line), and  
240 upper (110 m) ocean potential temperature anomaly (grey dashed line)<sup>56</sup>. Time-series are shown for (a)  
241 unnamed North Bone Bay), (b) Gavin Ice Piedmont, (c) Leonardo, (d) Hotine, (e) Trooz, (f) Keith, (g)  
242 Cadman and (h) Fleming Glaciers. Highlight glaciers a - f were selected based on their large seasonal  
243 ice speed variability (autocorrelation values of 0.648, 0.314, 0.586, 0.703, 0.575, 0.575 respectively),  
244 and to give a spread of locations along the west Antarctic Peninsula and show a range of faster and  
245 slower mean ice speeds.

246 **Figure 3 – Annual distribution of speed maximums and environmental forcings.**

247 (a) Histogram of the month of velocity maximum (reds) and velocity minimum (blue) on all glaciers  
248 (light shading) and top 20 glaciers by autocorrelation (dark shading). (b) West AP basin total modelled  
249 snowmelt plus rain (blue) and runoff (mauve) from RACMO 2.3p2<sup>43,52</sup> and monthly mean ocean  
250 temperature anomaly (°C) for all sample points (black dashed line)<sup>56</sup>. Both plots cover the period of full  
251 availability for all datasets: July 2016 – July 2020.

## 252 **Methods**

### 253 **Ice Velocity Observations**

254 We exploit 10,434 Sentinel-1a and -1b Synthetic Aperture Radar (SAR) image pairs acquired over the  
255 west AP from December 2014 to May 2021. To improve data processing efficiency, every  
256 Interferometric Wide (IW) swath mode Single Look Complex (SLC) image was cropped to the  
257 dimensions of the drainage basin for each glacier (Fig. S1a)<sup>70,73</sup>, before the displacement of surface  
258 features was tracked using the intensity cross-correlation technique<sup>20,74</sup>. Velocity tracking on the AP is

259 particularly challenging because of the steeply sloping terrain, the small size of the glaciers (56.6 % in  
260 our study are less than 3 km wide near the terminus), and the extreme weather conditions including high  
261 snowfall and surface melt which alter the radar backscatter amplitude over the 6 or 12-day temporal  
262 baseline for each pair. This increases the difficulty of recognizing and tracking the displacement of  
263 features in sequential images. Ice speed measurements were posted on a 100 m grid and a spatially  
264 variable velocity error (Fig. S2a) was calculated by multiplying the signal to noise ratio of the cross-  
265 correlation with the ice speed (Fig. 1a)<sup>20,75</sup>.

### 266 **Time-Series of Ice Speed**

267 Ice speed time-series were extracted from 105 glaciers and their major tributaries from the tip of Trinity  
268 Peninsula to Sirocco Glacier in the South, in order to evaluate sub-annual change in velocity. Sample  
269 points were selected on glaciers up to  $-70^{\circ}$  S with a drainage area greater than  $50,000 \text{ km}^2$ <sup>70</sup>, excluding  
270 slow moving ice piedmonts or regions where radar shadow or layover prevents good measurement  
271 coverage (Fig. S1a). Points were located 1 km inland of the May 2021 calving front position or the most  
272 inland calving front on record to ensure that sample points were located on grounded ice while  
273 maximizing measurement coverage. The grounding line position of glaciers on the west Antarctic  
274 Peninsula is poorly known due to the difficulty in collecting measurements, lack of interferometric SAR  
275 coherence, and the steep topography with many small glaciers which must be individually  
276 characterized. The MEaSURES<sup>76</sup> and ASAID<sup>77</sup> grounding line datasets suggest that of our 8 highlight  
277 glaciers, Fleming (MEaSURES and ASAID), Trooz and Cadman (ASAID only) Glaciers have small  
278 floating ice tongues. For all 105 glaciers, points are all inland of the MEaSURES grounding line.

279 We used a single sample point rather than a larger region because of the narrow width of many glaciers  
280 on the west Antarctic Peninsula, with an average width at the terminus of 3.0 km across all 105 glaciers  
281 in the study region. We sensitivity tested these results by also extracting data from a 500 x 500 m and  
282 1100 x 1100 m grid, which showed a mean difference of -7.90 m/yr and -56.83 m/yr respectively,  
283 averaged across all glaciers on the west AP. The larger difference for the 1100 x 1100 m grid is  
284 attributed to be the impact of including data from off-glacier and slower flowing regions outside the  
285 main trunk on narrow glaciers. To assess whether the observed seasonal signal is sensitive to the choice

286 of sampling strategy, we compared the ice speed anomaly in the 3 sampling regimes. We find the mean  
287 difference in ice speed anomaly from the sample point data was 0.63 m/yr and -0.34 m/yr for the for  
288 500 x 500 m and 1100 x 1100 m grids respectively, showing that the magnitude and timing of ice  
289 velocity fluctuations is consistent.

290 A Bayesian recursive smoother<sup>78–80</sup> was applied to each ice velocity time-series to produce a daily speed  
291 estimate and corresponding uncertainty, while accounting for the measurement error, and statistics for  
292 each glacier were calculated from this dataset (Fig. S3). The result shows how this post-processing step  
293 significantly reduces the uncertainty on ice speed throughout the time series, enabling speed change  
294 signals to be more clearly resolved above the measurement noise.

### 295 **Impact of Radar Penetration on Ice Velocity Measurements**

296 Radar instruments penetrate the glacier's snowpack, unlike optical or laser instruments which use  
297 visible light and therefore reflect off the snow surface. The depth that the radar penetrates (otherwise  
298 known as the scattering horizon) can vary in both space and time, but is primarily affected by the density  
299 of the snowpack and the presence of liquid meltwater. When there is surface melt the scattering horizon  
300 will raise closer to the snow surface, which given the side looking geometry of the radar instrument can  
301 induce an apparent small change in horizontal motion in the radar line of sight. As this is not related to  
302 the displacement of ice, this horizontal motion is a processing artefact and should not be misinterpreted  
303 as a real change in ice speed. This artefact only affects the range direction (line-of-sight) component of  
304 the 2D velocity field, not the azimuth (along track component); and it can only occur when there is a  
305 difference in the scattering horizon between two images - i.e. once the scattering horizon has raised (or  
306 lowered) there will be no artefact in the velocity measurement. Previous studies<sup>49</sup> have discussed the  
307 possible impact of a surface melt induced, radar scattering horizon effects on ice velocity measurements  
308 from SAR data, specifically in relation to short-lived (6-day) acceleration events on the AP<sup>48</sup>.

309 There are a number of reasons why it is unlikely that the speed change reported in this study is impacted  
310 by radar scattering horizon processing artefacts. Firstly, our results (Fig. S3), show that increased speeds  
311 are observed over a sustained period, approximately three months in the summer, which given the

312 weekly repeat observations equates to approximately 15 independent measurements clearly  
313 documenting the increase and decrease in speed. Such increases and decreases in speed over several  
314 successive measurements could not be caused by a radar scattering horizon effect. Secondly, previous  
315 studies<sup>49</sup> have shown that the look direction of the image acquisition will influence the sign (and  
316 magnitude) of the speed change attributed to a scattering horizon induced artefact. For example, due to  
317 the East-West look direction of Sentinel-1 acquisitions in the northern AP region, summer melting  
318 would induce a speed decrease by raising the radar scattering horizon on glaciers on the west AP  
319 coastline such as Cayley Glacier<sup>49</sup>, however, we observe summertime acceleration in the same region.  
320 We also make use of ice velocity tracking data from multiple Sentinel-1 frames and viewing angles  
321 across the study area and in some cases for the same glacier if it is covered by multiple frames, thereby  
322 reducing the impact of geometry influenced processing artefacts should they be present. Finally, as  
323 described above, we use a Bayesian recursive smoother to produce the most likely estimate for ice speed  
324 in our time series given the measurement error<sup>20,75</sup> therefore, our results are significantly less susceptible  
325 to individual anomalous velocity tracking results.

### 326 **Statistical Assessment of Ice Speed Periodicity**

327 We used a statistical assessment to determine the magnitude and periodicity of intra-annual speed  
328 variations in the Bayesian smoothed time-series from all 105 west AP glaciers (Fig. 2). Each Bayesian  
329 smoothed ice speed time-series was detrended using a third order polynomial to remove multi-year  
330 signals, then divided into yearly segments from 1<sup>st</sup> July to 30<sup>th</sup> June. Within each year, we take the total  
331 variability (minimum to maximum) and inter-quartile range (IQR) of the time-series in absolute terms  
332 and normalized as a percentage of the mean speed. We assessed the annual self-similarity of each speed  
333 time-series by calculating the autocorrelation at lags of 1 to 5-years, and we calculated the mean of  
334 these yearly autocorrelation values to give a single statistic per-glacier for the whole 6-year study  
335 period. High autocorrelation values indicate that a glacier has strong annual periodicity in its ice speed  
336 time-series, whereas the IQR indicates that the corresponding glacier has a large amplitude speed  
337 variability. This method was chosen over other frequency-based analyses as it requires no prior  
338 assumptions about the shape of the signal's waveform.

339 The formula used for autocorrelation for lag  $k$  is:

$$340 \quad r_k = \frac{c_k}{c_0} * \frac{T - k}{T}$$

$$341 \quad c_k = \frac{1}{T} \sum_{t=1}^{T-k} (y_t - \bar{y})(y_{t-k} - \bar{y})$$

342 Where  $T$  is the number of samples in the time series,  $c_0$  is the sample variance, as defined in previous  
343 work<sup>81</sup>.

### 344 **Environmental Forcing Data**

345 To investigate the availability of surface water on the west AP during the study period we extracted  
346 daily estimates of snowmelt and rainfall from the RACMO2.3p2 regional climate model (Fig. 2)<sup>43,52</sup>.  
347 While the spatial resolution of the regional climate model is relatively high (5.5 km), the small size of  
348 the glaciers in the AP study region may limit the accuracy with which the climatology of an individual  
349 glacier can be resolved. We combine both rainfall and snowmelt data as these variables represent liquid  
350 water availability at different times of the summer, and have been shown to impact the speed of ice flow  
351 in Greenland<sup>82</sup>. The surface hydrology data provides a reliable estimate of the onset, magnitude, and  
352 duration of the annually variable summer melt season, and enables differences in the spatial pattern to  
353 be resolved along the 1000 km-long west AP coast.

354 We used the GLORYS12V1 European Commission (EC) Copernicus Marine Service global ocean  
355 eddy-resolving (1/12° horizontal resolution, 50 vertical levels) reanalysis model<sup>56</sup> to evaluate ocean  
356 temperature variability in the Bellingshausen Sea, between 2014 and 2021 (Fig. 1b, Fig. 2). While ice  
357 thickness at the grounding line is highly uncertain on the AP due to the complex terrain and a paucity  
358 of bed elevation measurements, we aim to assess the temperature variability of ocean water in contact  
359 with the ice. We extracted monthly potential temperature data in the region between our ice speed  
360 sample points and 30 km offshore, or as far as islands and channels would allow. The depth averaged  
361 temperature anomaly in the top 110 m of the water column was then calculated relative to the 2015 to  
362 2020 mean, and we detrended the upper-ocean temperature anomaly time-series using a third order

363 polynomial fit to remove any long-term trend in ocean heat change. This depth is chosen to capture  
364 temperature fluctuations on a seasonal scale; to give fair comparison where glacier grounding depths  
365 are largely unknown. Previous studies in other regions have shown that glacier frontal ablation rates are  
366 strongly correlated with ocean temperature at a depth of 20-60 m<sup>62</sup>. Finally, we measured the  
367 interquartile range for each complete year and averaged this to give a single seasonal ocean temperature  
368 variability value per grid cell, which provides information on the on the inter-annual, seasonal ocean  
369 temperature variability (Fig. 1b).

### 370 **Calving Front Location**

371 We measured the change in calving front position on eight highlight glaciers with significant speed  
372 variability, by manually digitizing the terminus location in Sentinel-1 images using the GEEDiT  
373 digitization tool (Fig. 2)<sup>59</sup>. Time-series were produced at the highest spatiotemporal resolution possible  
374 by digitizing the whole archive of ~weekly Sentinel-1 images for each of these glaciers, at the resolution  
375 of the Sentinel-1 Ground Range Detected (GRD) product ( $\pm 10$  m). Change in terminus position was  
376 calculated using a curvilinear box with a 1 km width using the MaQiT tool.

### 377 **Ice Discharge Budget and Mass Balance Estimates**

378 We calculate ice discharge from selected glaciers by integrating ice velocity across a flux gate defined  
379 at 1 km inland from the terminus, to ensure ice speed is extracted from the grounded ice. Flow  
380 direction is taken from the MEaSURES ice speed mosaic dataset<sup>83</sup> and ice thickness was calculated  
381 from the difference between the bed elevation<sup>39</sup> and the ice surface elevation<sup>71</sup>. We assume a constant  
382 surface elevation during our study period, however, we apply a time varying firn air content  
383 correction from the RACMO 2.3p2 27 km firn densification model<sup>52</sup>. Ice discharge was calculated  
384 using the fully integrated time series from 1<sup>st</sup> Jan 2016 to 31<sup>st</sup> December 2020, followed by an ice  
385 discharge estimate using summertime only ice speeds, which was calculated by linearly interpolating  
386 ice speed between annual summer maximums (Table S1). Surface mass balance was calculated from  
387 RACMO 2.3p2 Antarctic Peninsula 5.5 km<sup>43,84</sup>, using drainage basins defined by Cook<sup>70</sup>. For Hotine  
388 glacier (Fig 2d), we calculate surface mass balance for the shared Hotine/Leay glacier drainage basin.



## 389 **Acknowledgements**

390 This work was led by the School of Earth and Environment at the University of Leeds. Data processing  
391 was undertaken on ARC3, part of the High-Performance Computing facilities at the University of  
392 Leeds, UK. The authors gratefully acknowledge the European Space Agency and the European  
393 Commission for the acquisition and availability of Sentinel-1 data and the use of datasets produced  
394 through the Copernicus Marine Service. We also acknowledge the Polar Geospatial Centre at the  
395 University of Minnesota for the availability of the REMA DEM and James Lea of the University of  
396 Liverpool for the public availability of the GEEDiT and MaQiT digitization tools. B.J.W. is supported  
397 by the Panorama Natural Environment Research Council (NERC) Doctoral Training Partnership (DTP),  
398 under grant NE/S007458/1. A.E.H. and B.J.D. are supported by the NERC DeCAdeS project  
399 (NE/T012757/1) and ESA Polar+ Ice Shelves project (ESA-IPL-POE-EF-cb-LE-2019-834). M.vd.B.  
400 was supported by the Netherlands Earth System Science Centre (NESSC). J.M.V.W. was supported by  
401 the NWO (Netherlands Organisation for Scientific Research) VENI grant VI.Veni.192.083. The authors  
402 would also like to thank the editor, James Super and the 3 referees for their comments which improved  
403 this manuscript.

## 404 **Author Contributions**

405 B.J.W. and A.E.H. designed this study. B.J.W. processed the ice velocity data from the Sentinel-1  
406 imagery and performed the analysis on all datasets. J.M.v.W. and M.vd.B. produced the regional climate  
407 model data. B.J.D. extracted the ocean temperature data. B.J.W. and A.E.H. wrote the manuscript. All  
408 authors contributed to scientific discussion, interpretation of the results and contributed to the  
409 manuscript.

## 410 **Competing Interests**

411 The authors declare no competing interests.

## 412 **Data Availability**

413 Source data used in this study are available as follows: Copernicus Sentinel-1A/B is available directly  
414 from the European Space Agency (<https://scihub.copernicus.eu/>). Copernicus Marine Service  
415 GLORYS12V1 global ocean physics reanalysis data (<https://doi.org/10.48670/moi-00021>). REMA  
416 Antarctic digital elevation model V1 (<https://doi.org/10.7910/DVN/SAIK8B>), International  
417 Bathymetric Chart of the Southern Ocean V1.0 ([https://ibcso.org/previous\\_releases/](https://ibcso.org/previous_releases/),  
418 <https://doi.org/10.1002/grl.50413>), glacier basin inventory  
419 (<https://doi.org/10.1017/S0954102014000200>)

420 Data produced during this study are available at: (<https://doi.org/10.5281/zenodo.7521416>). This  
421 includes: Ice speed time series for all glaciers, calving front positions for 8 highlight glaciers, glacier  
422 drainage basin scale ice velocity for 8 highlight glaciers, RACMO regional climate model data.

## 423 **References**

- 424 1. Shepherd, A. *et al.* Mass balance of the Antarctic Ice Sheet from 1992 to 2017. *Nature*  
425 **558**, 219–222 (2018).
- 426 2. Slater, T., Hogg, A. E. & Mottram, R. Ice-sheet losses track high-end sea-level rise  
427 projections. *Nat. Clim. Change* **10**, 879–881 (2020).
- 428 3. Dutrieux, P. *et al.* Strong Sensitivity of Pine Island Ice-Shelf Melting to Climatic  
429 Variability. *Science* **343**, 174–178 (2014).
- 430 4. Christianson, K. *et al.* Sensitivity of Pine Island Glacier to observed ocean forcing.  
431 *Geophys. Res. Lett.* **43**, 10,817–10,825 (2016).
- 432 5. Jenkins, A. *et al.* West Antarctic Ice Sheet retreat in the Amundsen Sea driven by decadal  
433 oceanic variability. *Nat. Geosci.* **11**, 733–738 (2018).
- 434 6. Reese, R., Albrecht, T., Mengel, M., Asay-Davis, X. & Winkelmann, R. Antarctic sub-  
435 shelf melt rates via PICO. *The Cryosphere* **12**, 1969–1985 (2018).

- 436 7. Gudmundsson, G. H., Paolo, F. S., Adusumilli, S. & Fricker, H. A. Instantaneous  
437 Antarctic ice sheet mass loss driven by thinning ice shelves. *Geophys. Res. Lett.* **46**,  
438 13903–13909 (2019).
- 439 8. Scambos, T. A., Bohlander, J. A., Shuman, C. A. & Skvarca, P. Glacier acceleration and  
440 thinning after ice shelf collapse in the Larsen B embayment, Antarctica. *Geophys. Res.*  
441 *Lett.* **31**, (2004).
- 442 9. Rignot, E. *et al.* Accelerated ice discharge from the Antarctic Peninsula following the  
443 collapse of Larsen B ice shelf. *Geophys. Res. Lett.* **31**, L18401 1-4 (2004).
- 444 10. Joughin, I., Shapero, D., Smith, B., Dutrieux, P. & Barham, M. Ice-shelf retreat drives  
445 recent Pine Island Glacier speedup. *Sci. Adv.* **7**, (2021).
- 446 11. Lhermitte, S. *et al.* Damage accelerates ice shelf instability and mass loss in Amundsen  
447 Sea Embayment. *Proc. Natl. Acad. Sci.* **117**, 24735–24741 (2020).
- 448 12. Rott, H., Müller, F., Nagler, T. & Floricioiu, D. The imbalance of glaciers after  
449 disintegration of Larsen-B ice shelf, Antarctic Peninsula. *The Cryosphere* **5**, 125–134  
450 (2011).
- 451 13. Rott, H. *et al.* Changing pattern of ice flow and mass balance for glaciers discharging into  
452 the Larsen A and B embayments, Antarctic Peninsula, 2011 to 2016. *The Cryosphere* **12**,  
453 1273–1291 (2018).
- 454 14. Mouginot, J., Rignot, E. & Scheuchl, B. Sustained increase in ice discharge from the  
455 Amundsen Sea Embayment, West Antarctica, from 1973 to 2013. *Geophys. Res. Lett.* **41**,  
456 1576–1584 (2014).
- 457 15. Alley, R. B., Clark, P. U., Huybrechts, P. & Joughin, I. Ice-Sheet and Sea-Level Changes.  
458 *Science* **310**, 456–460 (2005).
- 459 16. Barrand, N. E. *et al.* Computing the volume response of the Antarctic Peninsula ice sheet  
460 to warming scenarios to 2200. *J. Glaciol.* **59**, 397–409 (2013).

- 461 17. Cornford, S. L. *et al.* Century-scale simulations of the response of the West Antarctic Ice  
462 Sheet to a warming climate. *The Cryosphere* **9**, 1579–1600 (2015).
- 463 18. Rignot, E., Mouginot, J. & Scheuchl, B. Ice Flow of the Antarctic Ice Sheet. *Science* **333**,  
464 1427–1430 (2011).
- 465 19. Scambos, T. A., Berthier, E. & Shuman, C. A. The triggering of subglacial lake drainage  
466 during rapid glacier drawdown: Crane Glacier, Antarctic Peninsula. *Ann. Glaciol.* **52**, 74–  
467 82 (2011).
- 468 20. Selley, H. L. *et al.* Widespread increase in dynamic imbalance in the Getz region of  
469 Antarctica from 1994 to 2018. *Nat. Commun.* **12**, 1133 (2021).
- 470 21. Friedl, P., Seehaus, T. C., Wendt, A., Braun, M. H. & Höppner, K. Recent dynamic  
471 changes on Fleming Glacier after the disintegration of Wordie Ice Shelf, Antarctic  
472 Peninsula. *The Cryosphere* **12**, 1347–1365 (2018).
- 473 22. Pritchard, H. D. & Vaughan, D. G. Widespread acceleration of tidewater glaciers on the  
474 Antarctic Peninsula. *J. Geophys. Res. Earth Surf.* **112**, (2007).
- 475 23. Seehaus, T., Cook, A. J., Silva, A. B. & Braun, M. Changes in glacier dynamics in the  
476 northern Antarctic Peninsula since 1985. *The Cryosphere* **12**, 577–594 (2018).
- 477 24. Joughin, I. *et al.* Seasonal Speedup Along the Western Flank of the Greenland Ice Sheet.  
478 *Science* **320**, 781–783 (2008).
- 479 25. Moon, T. *et al.* Distinct patterns of seasonal Greenland glacier velocity. *Geophys. Res.*  
480 *Lett.* **41**, 7209–7216 (2014).
- 481 26. Moon, T., Joughin, I. & Smith, B. Seasonal to multiyear variability of glacier surface  
482 velocity, terminus position, and sea ice/ice mélange in northwest Greenland. *J. Geophys.*  
483 *Res. Earth Surf.* **120**, 818–833 (2015).
- 484 27. Sundal, A. V. *et al.* Melt-induced speed-up of Greenland ice sheet offset by efficient  
485 subglacial drainage. *Nature* **469**, 521–524 (2011).

- 486 28. Vijay, S. *et al.* Resolving Seasonal Ice Velocity of 45 Greenlandic Glaciers With Very  
487 High Temporal Details. *Geophys. Res. Lett.* **46**, 1485–1495 (2019).
- 488 29. Greene, C. A., Young, D. A., Gwyther, D. E., Galton-Fenzi, B. K. & Blankenship, D. D.  
489 Seasonal dynamics of Totten Ice Shelf controlled by sea ice buttressing. *The Cryosphere*  
490 **12**, 2869–2882 (2018).
- 491 30. Liang, Q. *et al.* Ice flow variations at Polar Record Glacier, East Antarctica. *J. Glaciol.*  
492 **65**, 279–287 (2019).
- 493 31. Boxall, K., Christie, F. D. W., Willis, I. C., Wuite, J. & Nagler, T. Seasonal land-ice-flow  
494 variability in the Antarctic Peninsula. *The Cryosphere* **16**, 3907–3932 (2022).
- 495 32. Cook, A. J. & Vaughan, D. G. Overview of areal changes of the ice shelves on the  
496 Antarctic Peninsula over the past 50 years. *The Cryosphere* **4**, 77–98 (2010).
- 497 33. Rott, H., Skvarca, P. & Nagler, T. Rapid Collapse of Northern Larsen Ice Shelf,  
498 Antarctica. *Science* **271**, 788–792 (1996).
- 499 34. Rack, W. & Rott, H. Pattern of retreat and disintegration of the Larsen B ice shelf,  
500 Antarctic Peninsula. *Ann. Glaciol.* **39**, 505–510 (2004).
- 501 35. Seehaus, T. C. *et al.* Dynamic Response of Sjögren Inlet Glaciers, Antarctic Peninsula, to  
502 Ice Shelf Breakup Derived from Multi-Mission Remote Sensing Time Series. *Front.*  
503 *Earth Sci.* **4**, (2016).
- 504 36. Brachfeld, S. *et al.* Holocene history of the Larsen-A Ice Shelf constrained by  
505 geomagnetic paleointensity dating. *Geology* **31**, 749–752 (2003).
- 506 37. Pudsey, C. J. & Evans, J. First survey of Antarctic sub-ice shelf sediments reveals mid-  
507 Holocene ice shelf retreat. *Geology* **29**, 787–790 (2001).
- 508 38. Domack, E. *et al.* Stability of the Larsen B ice shelf on the Antarctic Peninsula during the  
509 Holocene epoch. *Nature* **436**, 681–685 (2005).

- 510 39. Huss, M. & Farinotti, D. A high-resolution bedrock map for the Antarctic Peninsula. *The*  
511 *Cryosphere* **8**, 1261–1273 (2014).
- 512 40. Shepherd, A. *et al.* Trends in Antarctic Ice Sheet Elevation and Mass. *Geophys. Res. Lett.*  
513 **46**, 8174–8183 (2019).
- 514 41. Vaughan, D. G. & Doake, C. S. M. Recent atmospheric warming and retreat of ice  
515 shelves on the Antarctic Peninsula. *Nature* **379**, 328–331 (1996).
- 516 42. Turner, J. *et al.* Absence of 21st century warming on Antarctic Peninsula consistent with  
517 natural variability. *Nature* **535**, 411–415 (2016).
- 518 43. van Wessem, J. M. *et al.* The modelled surface mass balance of the Antarctic Peninsula at  
519 5.5 km horizontal resolution. *The Cryosphere* **10**, 271–285 (2016).
- 520 44. Barrand, N. E. *et al.* Trends in Antarctic Peninsula surface melting conditions from  
521 observations and regional climate modeling. *J. Geophys. Res. Earth Surf.* **118**, 315–330  
522 (2013).
- 523 45. van Wessem, J. M., Meredith, M. P., Reijmer, C. H., van den Broeke, M. R. & Cook, A.  
524 J. Characteristics of the modelled meteoric freshwater budget of the western Antarctic  
525 Peninsula. *Deep Sea Res. Part II Top. Stud. Oceanogr.* **139**, 31–39 (2017).
- 526 46. Cook, A. J. *et al.* Ocean forcing of glacier retreat in the western Antarctic Peninsula.  
527 *Science* **353**, 283–286 (2016).
- 528 47. Hogg, A. E. *et al.* Increased ice flow in Western Palmer Land linked to ocean melting.  
529 *Geophys. Res. Lett.* **44**, 4159–4167 (2017).
- 530 48. Tuckett, P. *et al.* Rapid accelerations of Antarctic Peninsula outlet glaciers driven by  
531 surface melt. *Nat. Commun.* **10**, (2019).
- 532 49. Rott, H. *et al.* Impact of marine processes on flow dynamics of northern Antarctic  
533 Peninsula outlet glaciers. *Nat. Commun.* **11**, 2969 (2020).

- 534 50. Davison, B. J. *et al.* Subglacial Drainage Evolution Modulates Seasonal Ice Flow  
535 Variability of Three Tidewater Glaciers in Southwest Greenland. *J. Geophys. Res. Earth*  
536 *Surf.* **125**, (2020).
- 537 51. Konrad, H. *et al.* Uneven onset and pace of ice-dynamical imbalance in the Amundsen  
538 Sea Embayment, West Antarctica. *Geophys. Res. Lett.* **44**, 910–918 (2017).
- 539 52. van Wessem, J. M. *et al.* Modelling the climate and surface mass balance of polar ice  
540 sheets using RACMO2 – Part 2: Antarctica (1979–2016). *The Cryosphere* **12**, 1479–1498  
541 (2018).
- 542 53. Veldhuijsen, S. B. M., van de Berg, W. J., Brils, M., Kuipers Munneke, P. & van den  
543 Broeke, M. R. Characteristics of the contemporary Antarctic firn layer simulated with  
544 IMAU-FDM v1.2A (1979–2020). *Cryosphere Discuss.* 1–26 (2022)  
545 doi:10.5194/tc-2022-118.
- 546 54. van Wessem, J. M., Steger, C. R., Wever, N. & van den Broeke, M. R. An exploratory  
547 modelling study of perennial firn aquifers in the Antarctic Peninsula for the period 1979–  
548 2016. *The Cryosphere* **15**, 695–714 (2021).
- 549 55. Banwell, A. F. *et al.* The 32-year record-high surface melt in 2019/2020 on the northern  
550 George VI Ice Shelf, Antarctic Peninsula. *The Cryosphere* **15**, 909–925 (2021).
- 551 56. Jean-Michel, L. *et al.* The Copernicus Global 1/12° Oceanic and Sea Ice GLORYS12  
552 Reanalysis. *Front. Earth Sci.* **9**, 585 (2021).
- 553 57. Stammerjohn, S. E., Martinson, D. G., Smith, R. C. & Iannuzzi, R. A. Sea ice in the  
554 western Antarctic Peninsula region: Spatio-temporal variability from ecological and  
555 climate change perspectives. *Deep Sea Res. Part II Top. Stud. Oceanogr.* **55**, 2041–2058  
556 (2008).

- 557 58. Venables, H. J. & Meredith, M. P. Feedbacks between ice cover, ocean stratification, and  
558 heat content in Ryder Bay, western Antarctic Peninsula. *J. Geophys. Res. Oceans* **119**,  
559 5323–5336 (2014).
- 560 59. Lea, J. M. The Google Earth Engine Digitisation Tool (GEEDiT) and the Margin change  
561 Quantification Tool (MaQiT) &ndash; simple tools for the rapid mapping and  
562 quantification of changing Earth surface margins. *Earth Surf. Dyn.* **6**, 551–561 (2018).
- 563 60. Howat, I. M., Joughin, I., Fahnestock, M., Smith, B. E. & Scambos, T. A. Synchronous  
564 retreat and acceleration of southeast Greenland outlet glaciers 2000–06: ice dynamics and  
565 coupling to climate. *J. Glaciol.* **54**, 646–660 (2008).
- 566 61. Frank, T., Åkesson, H., de Fleurian, B., Morlighem, M. & Nisancioglu, K. H. Geometric  
567 controls of tidewater glacier dynamics. *The Cryosphere* **16**, 581–601 (2022).
- 568 62. Luckman, A. *et al.* Calving rates at tidewater glaciers vary strongly with ocean  
569 temperature. *Nat. Commun.* **6**, 8566 (2015).
- 570 63. Dryak, M. C. & Enderlin, E. M. Analysis of Antarctic Peninsula glacier frontal ablation  
571 rates with respect to iceberg melt-inferred variability in ocean conditions. *J. Glaciol.* **66**,  
572 457–470 (2020).
- 573 64. Rodrigo, C., Giglio, S. & Varas, A. Glacier sediment plumes in small bays on the Danco  
574 Coast, Antarctic Peninsula. *Antarct. Sci.* **28**, 395–404 (2016).
- 575 65. Rodrigo, C., Varas-Gómez, A., Bustamante-Maino, A. & Mena-Hodges, E. High-  
576 concentration sediment plumes, Horseshoe Island, western Antarctic Peninsula. *Antarct.*  
577 *Sci.* **33**, 213–216 (2021).
- 578 66. Turner, J. *et al.* Antarctic climate change during the last 50 years. *Int. J. Climatol.* **25**,  
579 279–294 (2005).
- 580 67. Siegert, M. *et al.* The Antarctic Peninsula Under a 1.5°C Global Warming Scenario.  
581 *Front. Environ. Sci.* **7**, 102 (2019).



- 582 68. Trusel, L. D. *et al.* Divergent trajectories of Antarctic surface melt under two twenty-  
583 first-century climate scenarios. *Nat. Geosci.* **8**, 927–932 (2015).
- 584 69. Krinner, G., Magand, O., Simmonds, I., Genthon, C. & Dufresne, J.-L. Simulated  
585 Antarctic precipitation and surface mass balance at the end of the twentieth and twenty-  
586 first centuries. *Clim. Dyn.* **28**, 215–230 (2007).
- 587 70. Cook, A. J., Vaughan, D. G., Luckman, A. J. & Murray, T. A new Antarctic Peninsula  
588 glacier basin inventory and observed area changes since the 1940s. *Antarct. Sci.* **26**, 614–  
589 624 (2014).
- 590 71. Howat, I. M., Porter, C., Smith, B. E., Noh, M.-J. & Morin, P. The Reference Elevation  
591 Model of Antarctica. *The Cryosphere* **13**, 665–674 (2019).
- 592 72. Arndt, J. E. *et al.* The International Bathymetric Chart of the Southern Ocean (IBCSO)  
593 Version 1.0—A new bathymetric compilation covering circum-Antarctic waters.  
594 *Geophys. Res. Lett.* **40**, 3111–3117 (2013).
- 595

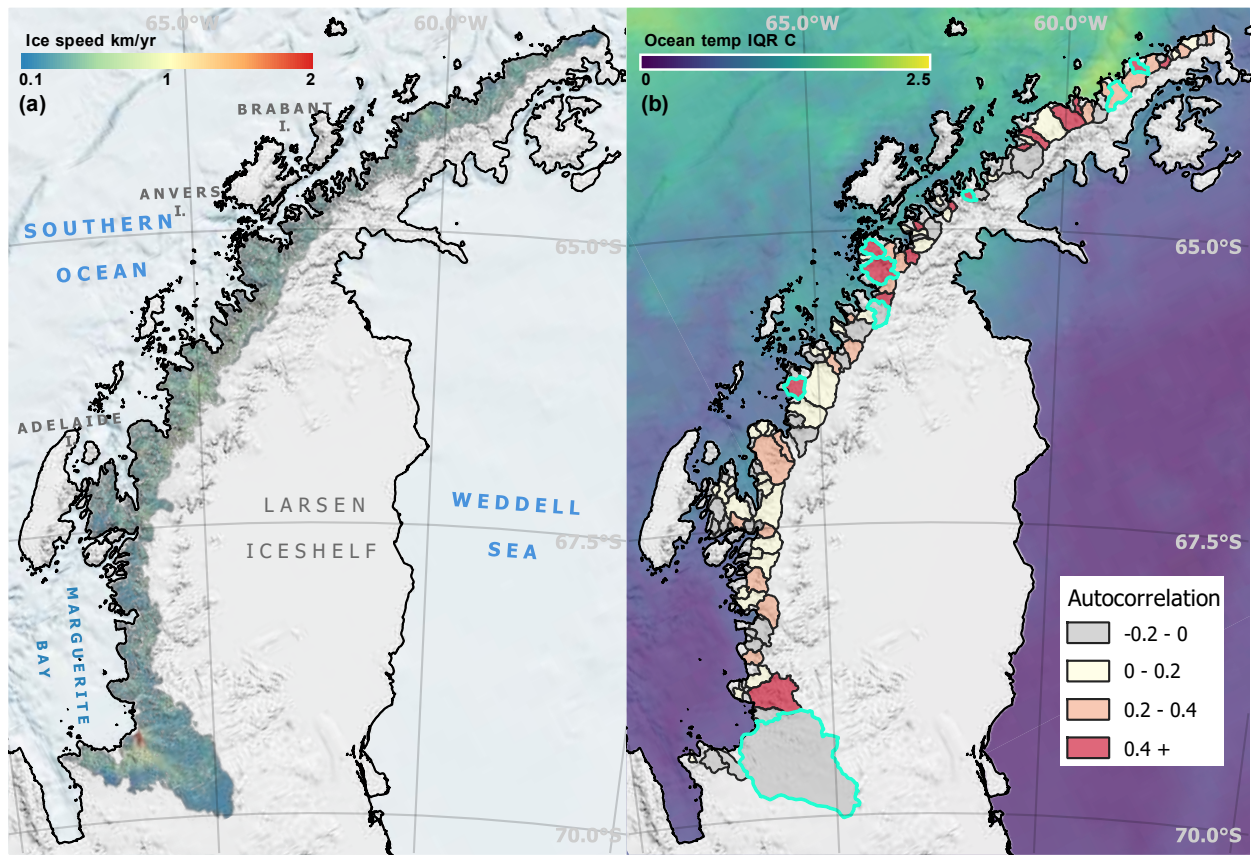
## 596 **Methods References**

- 597 73. Zwally, H. Jay, Mario B. Giovinetto, Matthew A. Beckley, and Jack L. Saba, 2012,  
598 Antarctic and Greenland Drainage Systems, GSFC Cryospheric Sciences Laboratory, at:  
599 [https://earth.gsfc.nasa.gov/cryo/data/polar-altimetry/antarctic-and-greenland-drainage-](https://earth.gsfc.nasa.gov/cryo/data/polar-altimetry/antarctic-and-greenland-drainage-systems)  
600 [systems](https://earth.gsfc.nasa.gov/cryo/data/polar-altimetry/antarctic-and-greenland-drainage-systems)
- 601 74. Strozzi, T., Luckman, A., Murray, T. & Wegmuller, U. Glacier Motion Estimation Using  
602 SAR Offset-Tracking Procedures. *Geosci. Remote Sens. IEEE Trans. On* **40**, 2384–2391  
603 (2002).
- 604 75. Lemos, A., Shepherd, A., McMillan, M. & Hogg, A. E. Seasonal Variations in the Flow  
605 of Land-Terminating Glaciers in Central-West Greenland Using Sentinel-1 Imagery.  
606 *Remote Sens.* **10**, 1878 (2018).

- 607 76. Rignot, Eric, J. Mouginot & B. Scheuchl. MEaSURES Antarctic Grounding Line from  
608 Differential Satellite Radar Interferometry, Version 2. (2016)  
609 doi:10.5067/IKBWW4RYHF1Q.
- 610 77. Bindschadler, R. *et al.* Getting around Antarctica: new high-resolution mappings of the  
611 grounded and freely-floating boundaries of the Antarctic ice sheet created for the  
612 International Polar Year. *The Cryosphere* **5**, 569–588 (2011).
- 613 78. Kalman, R. E. A New Approach to Linear Filtering and Prediction Problems. *J. Basic*  
614 *Eng.* **82**, 35–45 (1960).
- 615 79. Kalman, R. E. & Bucy, R. S. New Results in Linear Filtering and Prediction Theory. *J.*  
616 *Basic Eng.* **83**, 95–108 (1961).
- 617 80. Rauch, H. E., Tung, F. & Striebel, C. T. Maximum likelihood estimates of linear dynamic  
618 systems. *AIAA J.* **3**, 1445–1450 (1965).
- 619 81. Box, G. E. P., Jenkins, G. M. & Reinsel, G. C. *Time Series Analysis; Forecasting and*  
620 *Control.* (Prentice Hall, 1994).
- 621 82. Doyle, S. H. *et al.* Amplified melt and flow of the Greenland ice sheet driven by late-  
622 summer cyclonic rainfall. *Nat. Geosci.* **8**, 647–653 (2015).
- 623 83. Rignot, E., Mouginot, J. & Scheuchl, B. MEaSURES InSAR-Based Antarctica Ice  
624 Velocity Map, Version 2. (2017) doi:10.5067/D7GK8F5J8M8R.
- 625 84. Rignot, E. *et al.* Four decades of Antarctic Ice Sheet mass balance from 1979–2017.  
626 *Proc. Natl. Acad. Sci.* **116**, 1095–1103 (2019).

627

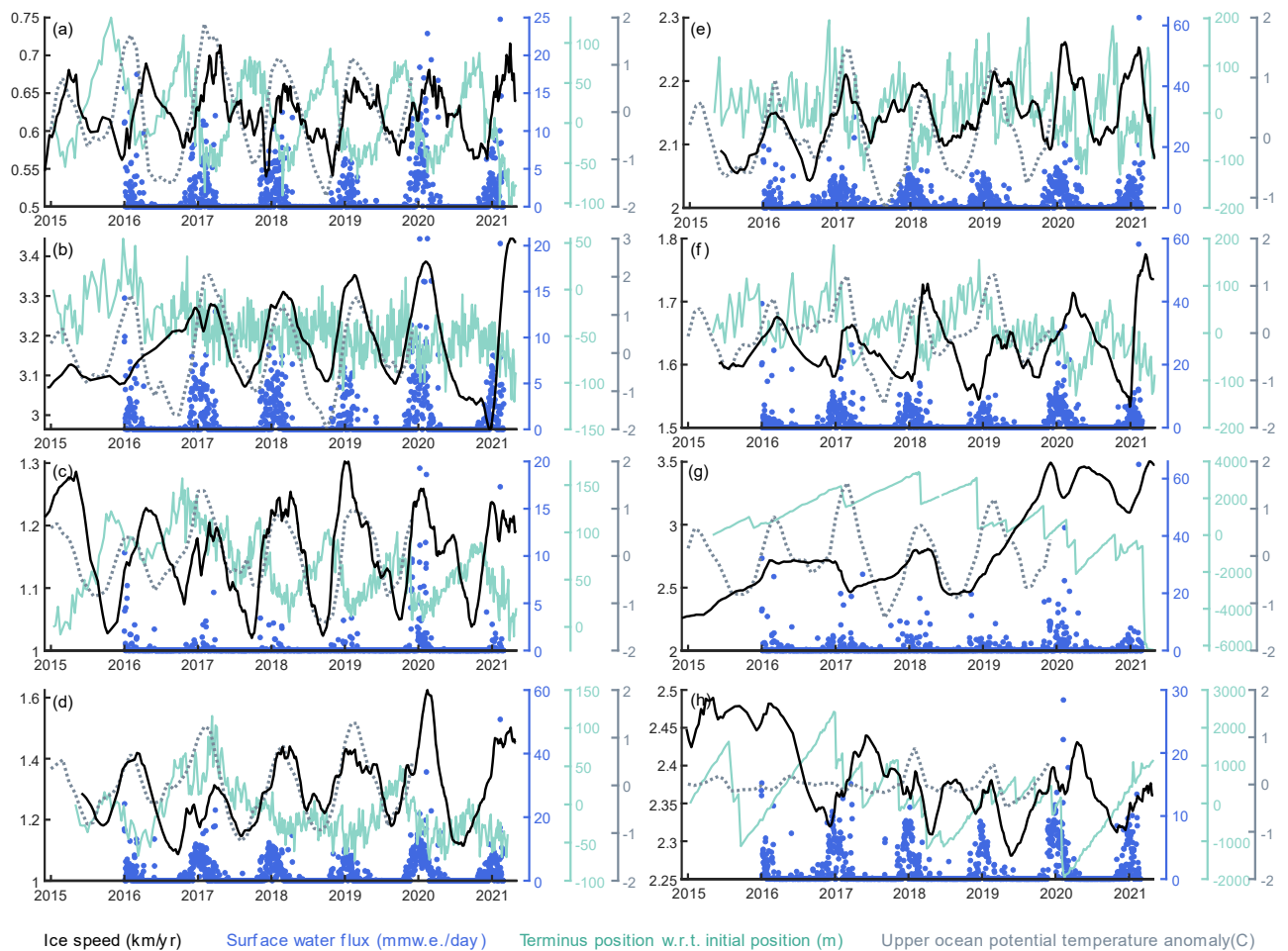
628



630

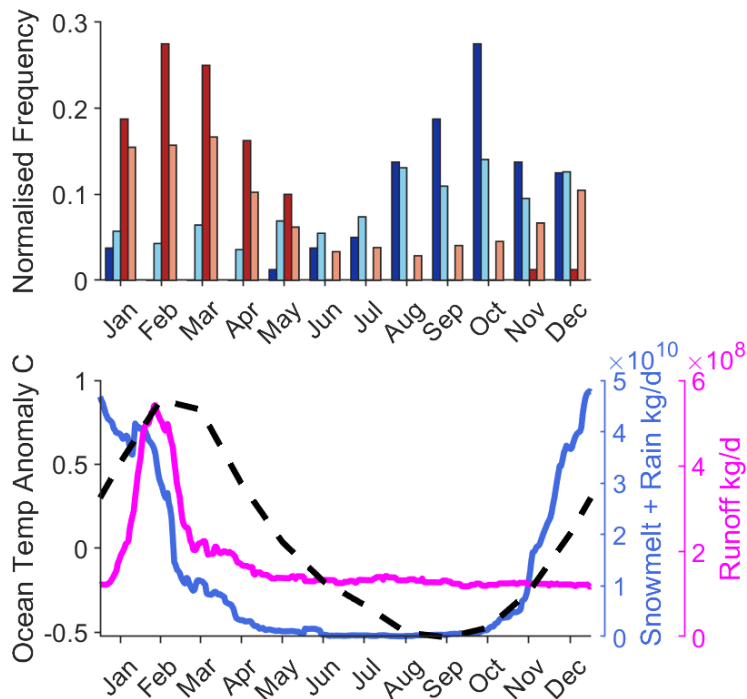
631 **Figure 1 – West Antarctic Peninsula ice speed map and ice speed autocorrelation.**

632 (a) Mean ice speed (km/yr) on the west Antarctic Peninsula (Dec 2014 – May 2021). (b) Glacier  
 633 drainage basins<sup>70</sup> shaded by the autocorrelation statistic (Dec 2014 – May 2021), which indicates high  
 634 (red) and low (light grey) annual periodicity in ice speed. Inter-annual upper ocean temperature  
 635 variation is also shown, measured as the annual interquartile range of the depth averaged temperature  
 636 anomaly from the top 110 m of the water column (2015 – 2020)<sup>56</sup>. The REMA Antarctica 200 m DEM  
 637 hill- shade<sup>71</sup>, coastline (black line) and hill-shade bathymetry from IBSCO v1<sup>72</sup> are shown on both maps  
 638 for illustrative purposes. Time -series are shown in Figure 2a-h for glaciers highlighted a-h.



640 **Figure 2a to h – Highlight glaciers time series of ice speed, surface water flux, terminus position**  
 641 **and ocean temperature anomaly.**

642 Time-series of Kalman smoothed ice speed (black solid line), RACMO2.3p2 surface water flux (snow  
 643 melt plus rain) (blue dots)<sup>43,52</sup> terminus position with respect to the final position (green solid line), and  
 644 upper (110 m) ocean potential temperature anomaly (grey dashed line)<sup>56</sup>. Time-series are shown for (a)  
 645 unnamed North Bone Bay), (b) Gavin Ice Piedmont, (c) Leonardo, (d) Hotine, (e) Trooz, (f) Keith, (g)  
 646 Cadman and (h) Fleming Glaciers. Highlight glaciers a - f were selected based on their large seasonal  
 647 ice speed variability (autocorrelation values of 0.648, 0.314, 0.586, 0.703, 0.575, 0.575 respectively),  
 648 and to give a spread of locations along the west Antarctic Peninsula and show a range of faster and  
 649 slower mean ice speeds.



650

651 **Figure 3 – Annual distribution of speed maximums and environmental forcings.**

652 (a) Histogram of the month of velocity maximum (reds) and velocity minimum (blue) on all glaciers  
 653 (light shading) and top 20 glaciers by autocorrelation (dark shading). (b) West AP basin total modelled  
 654 snowmelt plus rain (blue) and runoff (mauve) from RACMO 2.3p2<sup>43,52</sup> and monthly mean ocean  
 655 temperature anomaly (°C) for all sample points (black dashed line)<sup>56</sup>. Both plots cover the period of full  
 656 availability for all datasets: July 2016 – July 2020.